

Structure sensitivity of the methanation reaction: H₂-induced CO dissociation on nickel surfaces

M.P. Andersson^a, F. Abild-Pedersen^a, I.N. Remediakis^a, T. Bligaard^a, G. Jones^a, J. Engbæk^b,
O. Lytken^b, S. Horch^a, J.H. Nielsen^b, J. Sehested^c, J.R. Rostrup-Nielsen^c, J.K. Nørskov^a,
I. Chorkendorff^{b,*}

^a Center for Atomic-scale Materials Design (CAMD), Department of Physics, Nano-DTU, Building 307, Technical University of Denmark, 2800 Kgs. Lyngby, Denmark

^b Center for Individual Nanoparticle Functionality (CINF), Department of Physics, Nano-DTU, Building 312, Technical University of Denmark, 2800 Kgs. Lyngby, Denmark

^c Haldor Topsøe A/S, Nymøllevej 55, 2800 Kgs. Lyngby, Denmark

Received 19 October 2007; revised 19 December 2007; accepted 28 December 2007

Available online 15 February 2008

Abstract

The dissociation of CO serves both as a model test reaction on single crystals and as a relevant reaction step for industrial methanation. We combined extensive density functional theory calculations, ultra-high vacuum experiments on well-defined single crystals, and catalytic activity measurements on supported catalysts in a study of the dissociation mechanism of CO on Ni surfaces. We found that this process is highly structure-sensitive and also is sensitive to the presence of hydrogen: Under ultra-high vacuum, with no hydrogen present, the dissociation proceeds through a direct route in which only undercoordinated sites (e.g., steps) are active. Under methanation conditions, the dissociation also proceeds most favorably over undercoordinated sites, but through a COH species.

© 2008 Elsevier Inc. All rights reserved.

Keywords: Methanation; CO dissociation; Nickel catalyst; DFT

1. Introduction

The catalytic methanation reaction, $\text{CO} + 3\text{H}_2 \rightarrow \text{CH}_4 + \text{H}_2\text{O}$, has attracted considerable interest since it was reported by Sabatier [1]. This reaction is used in various industrial processes, including the removal of oxo-compounds (CO_x) in the feed gas for the ammonia synthesis [2], in connection with gasification of coal, where it can be used to produce methane from synthesis gas [3], and in relation to Fischer–Tropsch synthesis [4]. Another motivation for understanding this process in detail is purely scientific: It is one of the simplest catalytic reactions and serves as a test bed for our fundamental understanding of heterogeneous catalysis. Pioneering work by Goodman et al. [5–7] made the first comparison between surface

science single-crystal experiments [5] and supported Ni catalysts [8]. One of the conclusions from this work was that the methanation process proceeds with comparable rates per Ni atom on Ni(111) and Ni(100), as well as on supported Ni catalysts. It thus appears from these experiments that the reaction is structure-insensitive, whereas the reverse reaction, the steam reforming process, is structure-sensitive [9–13].

In this work, we address the influence of the surface structure on the CO activation on Ni. In general, the geometry of transition metal surface sites can have a profound impact on the dissociation probability of diatomic molecules. For example, NO has been found to dissociate preferentially on steps on Ru(0001) surfaces [14]. The same is true for N₂ dissociation, for which both theory and experiments have demonstrated a very large difference in reactivity between close packed surfaces and steps, corresponding to a difference in activation energy for dissociation of >1 eV [15,16]. Density functional theory (DFT) calculations have shown this to be true in nu-

* Corresponding author.

E-mail address: ibchork@fysik.dtu.dk (I. Chorkendorff).

merous cases [17–21], indicating that the step site should play an important role both in model systems and for supported nanoparticles [17].

When it comes to CO dissociation in low-pressure regime, Yates and coworkers elegantly used isotopic scrambling in temperature-programmed desorption (TPD) experiments on $^{12}\text{C}^{16}\text{O}$ and $^{13}\text{C}^{18}\text{O}$ on stepped Ru(109) under ultra-high vacuum (UHV) to demonstrate that CO dissociates only through the β -state related to steps [22,23], not on the flat Ru(0001) surface [24]. The same techniques were used in a study of CO dissociation on Ni(111), which found that CO desorbed rather than dissociated during a TPD experiment [25]. This is in agreement with previous work demonstrating no dissociation after TPD experiments on Ni(511) and Ni(100) by Benndorf and Meyer [26] and Goodman et al. [27], respectively. In contrast to these results, Nakano et al. used scanning tunneling microscopy (STM) to study the dissociation of CO on several stepped Ni(111) surfaces [28–30] and found that CO dissociated readily at 400 K [29]. This finding was also demonstrated by Lauritsen et al. using STM [31]. Based on these findings, it is obvious that the details of CO dissociation on Ni surfaces under UHV remain incompletely understood.

The conclusion that CO dissociation does not occur on Ni during TPD experiments [25–27], which is supported by the data presented later in this paper, indicates that the barrier for dissociation is larger than for desorption; that is, the dissociation barrier is $> \sim 1.2$ eV [32,33]. This is in disagreement with the activation energies as low as 1.0–1.1 eV found in studies of the kinetics of the methanation over both single crystals and catalysts at higher pressures [5–8,34,35]. Although there seems to be a reasonable consensus on the overall activation energy for the methanation reaction, this is not the case for the mechanism. Numerous works on supported nickel catalysts have considered the kinetics and the mechanism of the methanation process. For example, Coenen and co-workers [36] made an extensive study of the methanation reaction and evaluated several mechanisms; they found an excellent description by a model in which CH_x hydrogenation was assumed to be the rate-limiting step (RLS) and CO and hydrogen dissociation was assumed in equilibrium. This work was followed by a study by Klose and Baerns [37], who claimed that earlier work suffered from transport limitations and concluded that the RLS is hydrogenation of CH_2 . But these mechanisms were completely abandoned in a later work by Coenen et al. [38], who, through isotope labeling, determined that no scrambling occurred between labeled $^{12}\text{C}^{18}\text{O}$ and $^{13}\text{C}^{16}\text{O}$ [38] in the reaction mixture, thus proving the assumption of equilibrated dissociative adsorption of CO invalid. These authors instead introduced a new model that had been proposed earlier by Van Ho and Harriott [39] in which hydrogen-assisted CO dissociation was assumed to be the RLS. The predictions by the new model were in good agreement with the experimental data; thus, Coenen et al. concluded that either the CO or COH dissociation step could be the RLS [38]. DFT calculations support this picture [20,40]. In addition, Sehested et al. found that the methanation rate has a very low prefactor along with a low activation energy (1.01 eV) [35]. This is in very good agreement with the work on the methanation reaction by Goodman

and co-workers [5–7], who also observed such low prefactors and low activation energies of 1.07 eV both on single crystals and in comparison with rates measured on supported catalysts by Vannice [8,34]. In the single-crystal studies, only small differences (amounting to a factor of two) were found among the Ni(111) surface, the more open Ni(100) surface, and supported Ni catalysts. Because similar rates were found for the Ru(001) and Ru(110) surfaces [6,41] the reaction was deemed to be structure-insensitive, and the RLS was suggested to be an interplay of carbide deposition by the disproportionation reaction and carbide hydrogenation.

In this paper, we develop a consistent picture that describes the UHV results as well as the high-pressure catalyst data both qualitatively and semiquantitatively. This is obtained through DFT calculations, surface science experiments under UHV conditions, and comparison with experimental data reported here and in the literature on the methanation reaction.

2. DFT calculations

We performed DFT calculations on numerous different model surfaces displaying close-packed facets, steps, kinks, and double-step-sites modeling the edge sites on a finite size particle. Each surface is modeled by a slab with a thickness of three close-packed layers. Convergence was checked by also performing the DFT calculations for six instead of three Ni(111) layers. This led to a lowering of the barriers by only 0.03 eV. The adsorbates and the topmost Ni layer were allowed to relax fully in all configurations, and the calculations were performed with spin polarization included. All transition state energies were determined by increasing the bond lengths between C and O (for CO dissociation), C and OH (for C–OH dissociation), and CH and O (for HC–O dissociation) in small steps until a saddle point was reached.

All calculations were done using a plane-wave pseudopotential code and the RPBE exchange correlation functional [42]. Because we need to compare our results quantitatively to experimental findings, we included a recently proposed correction scheme [43,44]. We did this to avoid the well-known problem of overbinding when using DFT in combination with the generalized gradient approximation (GGA), which gives wrong site assignment for CO adsorption for many metals [45,46]. This correction is applied to all CO adsorption energies (and hence to all initial state energies for CO dissociation).

First, we considered in some detail Ni(111) surfaces with different defects. Figs. 1–4 display the results of the DFT calculations for four cases of CO dissociation: at low CO coverage, at low CO coverage with hydrogen present, at high CO coverage, and at high CO coverage with hydrogen present. DFT results for these four cases are collected in Table 1. The different surface structures are indexed using a letter (A–H).

Figs. 1 and 2 show (at low CO coverage), energies of the initial state of CO, the transition state, and the final state without and with the presence of hydrogen, respectively. Various different dissociation sites were considered (Table 1). At low CO coverage without hydrogen present, it was found that CO adsorbs most favorably over the kink site (see the insert in

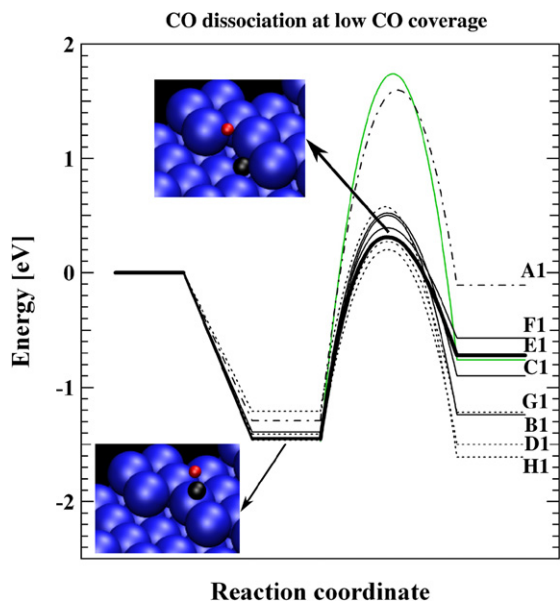


Fig. 1. Energy diagram for CO dissociation on Ni at low CO coverage corresponding to UHV conditions, showing CO adsorption and dissociation for various surface step- and edge structures (solid lines). The different structures investigated are nickel terrace sites, single steps, kinks and double steps. Each barrier is associated with an index referring to the actual surface structures, intermediates, and activation energies; notation is explained in Table 1. All results for double step structures and the Ni(100) are shown as dashed lines since these structures do not exist on a flat Ni(111) surface with only monatomic steps as seen in the STM images, see Fig. 9. The disproportionation reaction (Boudouard reaction) on the Ni(211) step is shown in green. The reaction route with the lowest reaction barrier (1.77 eV) under UHV conditions is pure CO dissociation on a Ni(321) surface (kink site, E1) and is shown with a bold line. The configuration of the CO molecule (carbon atom is black, oxygen atom is red) is shown along with the kink site for the initial and transition states. (For interpretation of the references to color in this figure legend the reader is referred to the web version of this article.)

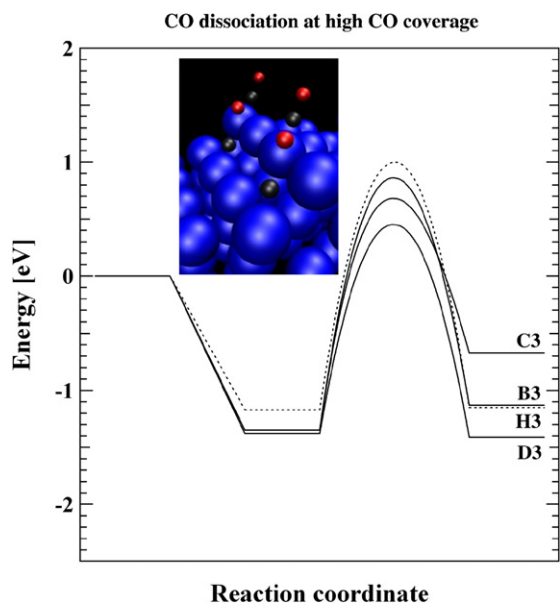


Fig. 3. Energy diagram for CO dissociation on Ni at high CO coverage (compare with Fig. 1). The most favorable reaction site is the double step site (D3) with an activation barrier of 1.92 eV only slightly higher than the barrier for CO dissociation at low pressures (1.7–1.9 eV). The transition state for the D3 structure is shown in the insert.

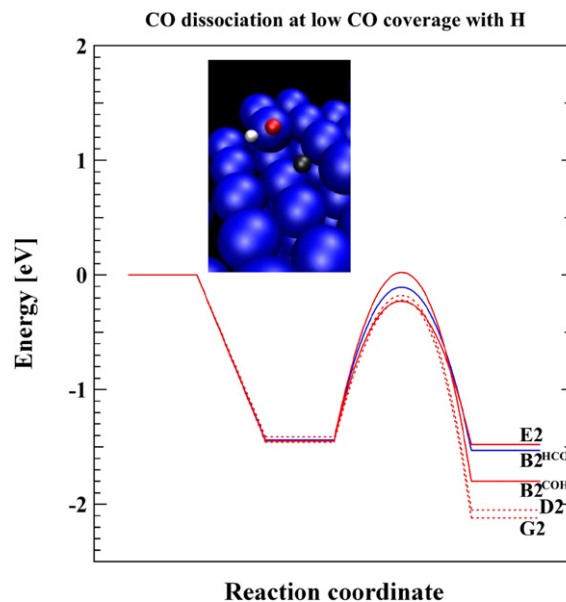


Fig. 2. Energy diagram for CO dissociation on Ni at low CO coverage, in the presence of H (compare with Fig. 1). Two mechanisms are considered: H induced dissociation via a COH intermediate (red) and via a HCO intermediate (blue). All results for double step structures are again shown as dashed lines. These structures do not exist on a flat Ni(111) surface with only monatomic steps as seen in the STM images, see Fig. 9. The activation is most favorable via COH over a kink site (1.22 eV, E2), but other undercoordinated sites are also active, see Table 1. The transition state for the E2 structure is shown in the insert (hydrogen atoms are white). (For interpretation of the references to color in this figure legend the reader is referred to the web version of this article.)

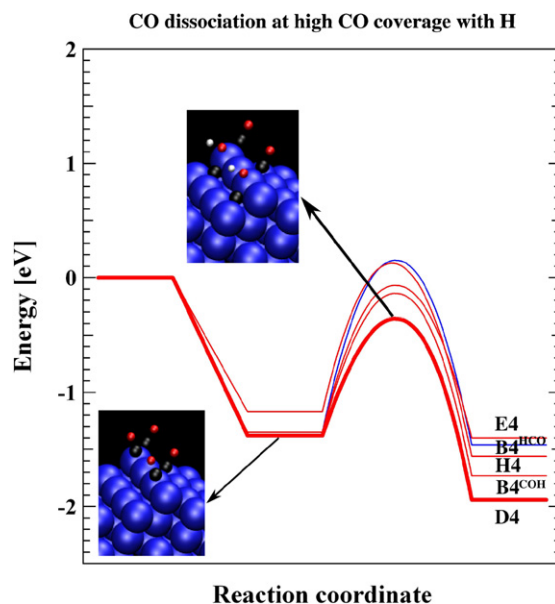


Fig. 4. Energy diagram for CO dissociation on Ni at high CO coverage, in the presence of H (compare with Fig. 1). These conditions correspond to methanation conditions over an industrial supported Ni catalyst. The two mechanisms via a COH intermediate (red) and via a HCO intermediate (blue) used in Fig. 2 are again considered. The reaction route with the lowest reaction barrier (1.08 eV) is dissociation via a COH intermediate on a Ni double step (D4) and is shown as a bold line. Nickel double steps serve as a model for edges as well as corners and these are certainly present on a supported catalyst. (For interpretation of the references to color in this figure legend the reader is referred to the web version of this article.)

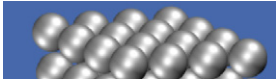
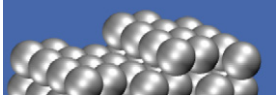
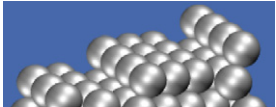
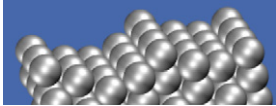
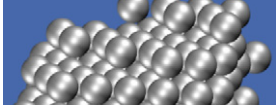
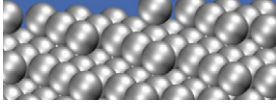
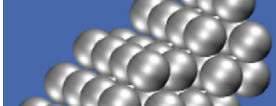
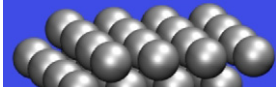
Fig. 1), which also offers a favorable transition state geometry for CO dissociation (see the insert) with an activation energy of 1.77 eV (Table 1, E1). At a double step, the activation energy was even lower (1.66 eV, D1), and at an ordinary step with no kinks, it was 1.91–1.94 eV (C1, B1). This should be compared with an activation energy for CO dissociation of 2.85 eV (A1) on a terrace site on Ni(111). Some other sites investigated displayed intermediate barrier heights (see Table 1). Because it also has been suggested that CO can dissociate through a disproportionation reaction [5], this possibility

was considered on step sites as well; this led to an activation energy of 3.2 eV, and thus this pathway was not considered further.

We conclude that in the absence of H, CO dissociation at defects with low coordination number was strongly favored over the close-packed Ni(111) surface and that the activation energy at the defects had a value of 1.7–1.9 eV. Furthermore, the transition state energy was located above the CO gas-phase energy, suggesting that CO will primarily desorb rather than dissociate in a TPD experiment.

Table 1

Collection of the calculated activation energies for the CO dissociation on a number of different surface structures. In order to visualize the details of the surface structure, only parts of the unit cell used for the calculation are shown here. The calculations consider low and high CO coverages and the absence and presence of hydrogen. The various reaction ensembles are indexed using a letter (A–H), describing the type of active site, and a number (1–4), describing the various reaction conditions, as explained in the table. This notation is used throughout the paper, in particular in Figs. 1–4. The values for E1 and D4 are shown in bold, as these are the relevant structures and activation energies for comparison to the UHV experiments and the methanation experiments, respectively

CO dissociation		E_a (eV)			
		1 low θ_{CO}	2 low θ_{CO} with H	3 high θ_{CO}	4 high θ_{CO} with H
A	 (111) terrace	2.85	–	–	–
B	 (211) step	1.94	1.33 (via HCO) 1.46 (via COH)	2.30	1.59 (via HCO) 1.30 (via COH)
C	 (221) step	1.91	–	2.12	–
D	 (311) double step	1.66	1.24 (via COH)	1.92	1.08 (via COH)
E	 (321) kink	1.77	1.22 (via COH)	–	1.37 (via COH)
F	 (431) kink	1.87	–	–	–
G	 (511) double step	1.68	1.23 (via COH)	–	–
H	 (100) terrace	1.87	1.21 (via COH)	2.17	1.29 (via COH)

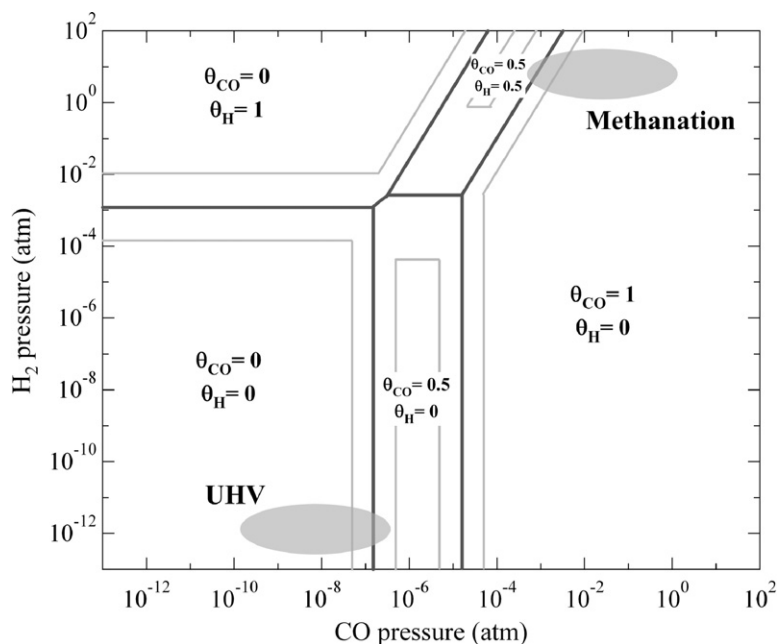


Fig. 5. The phase diagram shows the calculated edge configuration with the lowest free energy under various hydrogen and carbon monoxide pressures at 500 K. All energies are calculated using a two atom wide unit cell corresponding to Ni(211). The nearest neighbor interactions are taken into account via this approximation, and the entropy for gas phase species is included using standard formulas and the entropy for surface species is approximated using the harmonic vibrational entropy. Zero point energies are also included in the calculation of enthalpies. UHV and methanation conditions are indicated in the figure with grey areas. A black line between two or three different phases corresponds to an equal mixture of the neighboring phases whereas the grey lines are drawn parallel to the black lines and indicates that 75% of the surface is covered with the majority phase far from any triple point.

Investigating the effect of hydrogen first at low CO coverages (and pressures) requires knowledge of CO and H coverage at the reactive step site. Consequently, we constructed a phase diagram of the most dominant surface step configuration on Ni(211) (with a unit cell two atoms wide) as a function of CO and H₂ pressures through a statistical mechanics approach (Fig. 5). A temperature of 500 K (a typical methanation reaction temperature) was used. All entropies were calculated from the molecular partition functions. For gas-phase species, we included translational, rotational, and vibrational degrees of freedom and used standard thermodynamic expressions. Adsorbates were assumed to be tightly bound, and thus only vibrational degrees of freedom, again calculated using standard thermodynamic expressions, were included in the partition function. The harmonic approximation was used for all vibrations, and the zero-point energies thus obtained were included in the enthalpies. The relevant conditions for a UHV experiment and for the methanation reaction are indicated.

The phase diagram shows low H coverage at UHV conditions. For example, at a CO pressure of 6.7×10^{-9} atm (6.7×10^{-6} mbar) as used in the UHV experiment presented later in this paper, the calculated CO coverage is 0.02 and the H coverage is 10^{-5} . Fig. 2 shows the effect of hydrogen on the dissociation barrier of CO. Even though the H insertion mechanisms (via COH or HCO) have a lower effective activation energy ($E_{a,\text{COH}} = E_{\text{Transition state}} - E_{\text{CO ads.}} - (1/2)E_{\text{H}_2 \text{ gas}}$) of 1.22 eV (E2) than without hydrogen (1.77 eV for a kink site; E1), the free energy barrier is substantially higher due to the large loss of entropy at the very low hydrogen pressure; see the discussion that follows. This means that the calculations

suggest only a negligible effect of hydrogen in typical UHV experiments of CO dissociation. This is further confirmed by our experiments here and by previous work that attempted to hydrogenate CO with atomic hydrogen on Ru(109) without success [47].

At higher CO pressures corresponding to the region of the phase diagram in Fig. 5 in which the CO coverage along the step is close to 1 and the hydrogen coverage is close to 0, the CO molecule adsorbs most favorably in the bridge site at the steps. In this high CO coverage limit, dissociation barriers for CO are only slightly higher than the barriers in the low coverage limit (1.9–2.1 eV vs 1.7–1.9 eV; Fig. 3 and Table 1). Note that the site below the step has a considerably lower CO adsorption energy (by 0.45 eV, excluding CO–CO repulsion) than at the top of the step, and would be empty at the temperatures and pressures considered in Fig. 5.

The dissociation of CO at methanation conditions also involves high pressures of H₂, and, as discussed previously, it is possible that the presence of hydrogen could result in a lower barrier for dissociating CO. A reaction pathway over a COH intermediate was also recently suggested as an important route for the partial oxidation of methane over Rh(111) [48]. Therefore, we consider an additional type of mechanism in which the transition state for CO dissociation is stabilized by hydrogen (see Fig. 4) and thus the CO first reacts with adsorbed hydrogen, forming a COH intermediate, which then offers a lower activation barrier for the C–O bond dissociation. Two types of intermediates—the carbon–hydroxyl C–OH (red lines) and the formyl HC–O (blue lines)—are considered. We find that on a double-stepped Ni surface modeling an edge on a nanoparticle

(as shown in the insert in Fig. 4), hydrogen reduces the barrier significantly by causing C–O bond stretching as the CO–H intermediate forms. The resulting effective activation energy, $E_{a,\text{COH}}$ (defined above), is only 1.08 eV (Table 1, D4). At an ordinary step, it is a little higher, 1.30 eV (Table 1, B4). We also note that the hydrogenated HCO and COH intermediates are easily formed on nickel with activation barriers of ca. 0.8 eV, well below the desorption energy of CO of 1.24 eV [33], suggesting that COH can be considered in chemical equilibrium with adsorbed CO and H (and thus with gas-phase CO and H₂) under methanation conditions. We would not expect COH to be present on the surface in detectable amounts. We estimated the free energy difference between adsorbed COH and adsorbed CO and H₂ in the gas phase as 0.7 eV. The resulting COH coverage (at 500 K) was $<10^{-7}$ ML. We have not found any experimental identification of the adsorbed COH in the literature.

The activation of CO (by direct dissociation or via COH) is a key reaction step in the methanation reaction, and, as discussed in the Introduction, whether it is the RLS remains an open question. We can address this question computationally in the following way. We calculate the standard free energy of all relevant states (including transition states) in the reaction, as shown in Fig. 6. In such a free-energy diagram, the point with the highest (free) energy defines the slowest reaction step (at standard pressures). Fig. 6 shows the steps involving CO activation and the highest barrier for C hydrogenation (the last one forming CH₄) at different temperatures. The standard free energies for gas-phase species are calculated using statistical thermodynamics for a classical ideal gas. The Gibbs free energy for gas-phase species A at temperature T and pressure P is given by

$$G_A^{P,T} = E_A + E_{\text{ZPE}} + \Delta H^{0,T} - TS^T + RT \ln\left(\frac{P}{P^0}\right),$$

where E_A is the energy of gas-phase species A, E_{ZPE} is the zero-point energy, $\Delta H^{0,T}$ is the enthalpy change going from 0 K to temperature T , S^T is the entropy at temperature T , R is the universal gas constant, and P^0 is the standard pressure (taken to be 1 bar). A similar expression describes the free energy of species A adsorbed on a metal M,

$$G_{A^*}^{P,T} = E_{A^*} + E_{\text{ZPE}} + \Delta U^{0,T} - TS^T.$$

Here $E_{A^*} = E_{A/M} - E_M$, and the enthalpy change is replaced by a change in internal energy, $\Delta U^{0,T}$. Gas-phase entropies are taken from standard tables [49]. In the transition states, all real frequencies are included; thus, activation free energies give rates directly in harmonic transition state theory as

$$r = \frac{k_B T}{h} \exp\left(\frac{\Delta G_a}{k_B T}\right).$$

The vibrational frequencies used to determine E_{ZPE} , $\Delta U^{0,T}$, and S^T are also calculated using DFT; the results are given in Table 2. Two cases are shown in Fig. 6: at low CO coverage, where direct dissociation is dominant and hydrogenation can occur at the steps (a), and at high CO coverage, where

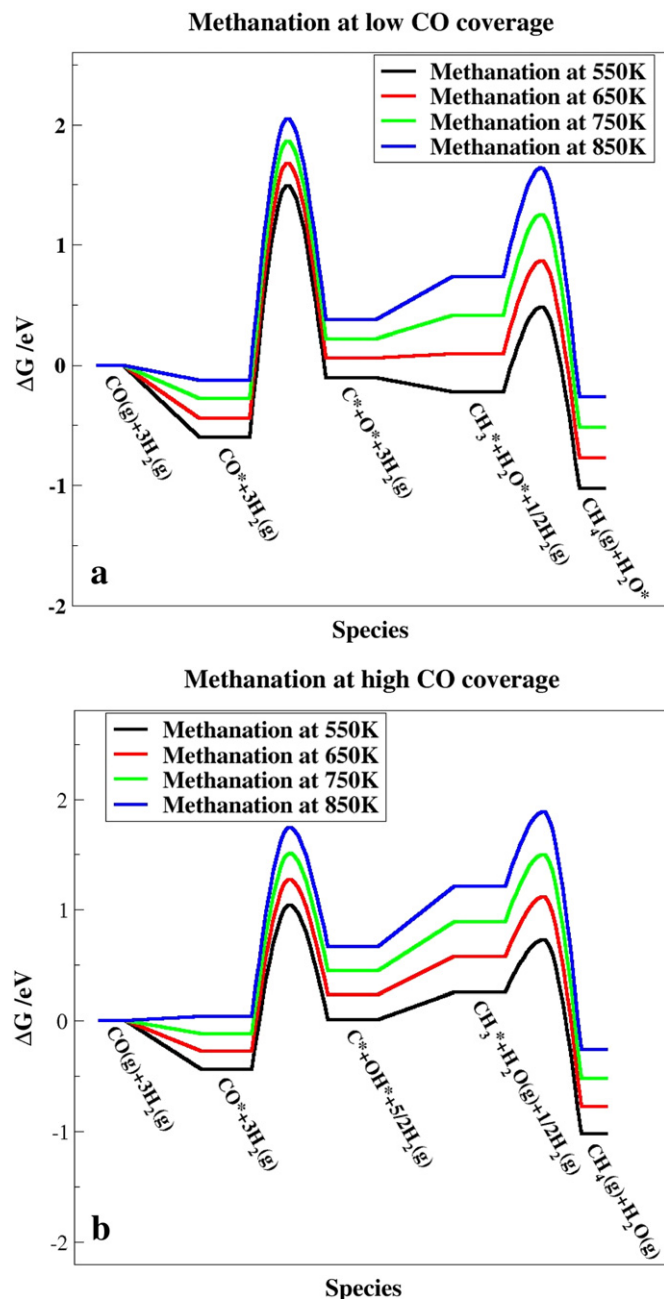


Fig. 6. Contracted free energy diagrams modeling the methanation reaction on a Ni(211) surface (Table 1, B) with low and high CO coverages at different temperatures (the 550 K diagram is shown lowest of the four and the 850 K is shown highest). The figure (a) shows the dissociation of CO in the low CO coverage regime. One clearly observes CO dissociation to be rate-limiting up to temperatures of at least 850 K. The figure (b) shows the dissociation in the high coverage regime. Here CO dissociation via COH is rate-limiting up until temperatures just below 850 K.

the process through COH is dominant and hydrogenation is blocked at the steps and must occur on the terraces (b).

Fig. 6 shows that at low temperatures, CO activation is the RLS in both processes. At higher temperatures (above those used in the methanation process), carbon hydrogenation becomes the RLS. This shift in RLS can explain a large part of the discrepancies among the various experimental studies, as we discuss later. For the moment, we conclude that the calculations

Table 2

The table shows vibrational data for the relevant intermediates in the methanation reaction. All data have been calculated using DFT except for the gas phase species here the vibrational frequencies were taken from Ref. [49]. Both ΔH and ΔS for the gas phase species have been calculated using the Shomate equation, for which the parameters can be found in Ref. [49]

Species	Vibrational modes (1/cm)		
CO*	1888	346	323
	287	214	160
COH*	3761	1254	1080
	456	435	385
	200	148	142
CH ₃ *	3092	3007	2519
	1385	1262	1200
	592	562	410
	204	195	86
CH ₃ *TS	3094	3021	2224
	1937	1442	1312
	1287	948	809
	441	200	170
	139	105	
CO*TS	579	516	453
	449	363	
COH*TS	3799	704	637
	579	498	296
	216	131	
CH ₄ (g)	3019	2917	1534
	1306		
CO(g)		2169.81	
H ₂ (g)		4401.21	

support the notion that under typical methanation conditions, CO activation (through COH) is the RLS.

All of the results presented so far are for species adsorbed on the step edge only. On a real nanoparticle catalyst, however, adsorption on the facets adjacent to the active edge site also could have a significant affect. Consequently, we investigated CO dissociation (via the COH intermediate) on the Ni(311) double step with full CO coverage along the step and either CO or H co-adsorbed on the (100) facet. The activation energy turned out to be only weakly influenced by the presence of CO or H on the adjacent (100) facet and to change by -0.02 eV with co-adsorbed CO and by $+0.04$ eV with co-adsorbed H. Thus, coverages of up to 0.5 of CO and/or H on the (100) facets is highly unlikely to have a major influence on the dissociation rate of CO on the active site.

For completeness, we also considered CO activation on Ni(100) surfaces (H1–4 in Table 1). At low CO coverage, the barriers for CO activation with or without H are as low as at the steps on Ni(111). The energy of the transition state, as well as the energy of the initial state for CO dissociation, is ~ 0.2 eV higher than at the double step on Ni(111) (D1); in fact, the geometries are very similar, the main difference being that at the double step, the step atoms have higher lying d -states and hence interact stronger with the CO. On the other hand, at the highest coverage possible at the CO partial pressures relevant to methanation (half a monolayer), the barrier for direct CO dissociation on Ni(100) is high (2.17 eV; see H3 in Table 1). The COH mechanism has a low barrier on Ni(100) even at high CO coverage (H4 in Table 1). But this surface cannot adsorb H atoms at these coverages. This is illustrated in Fig. 7, which shows that at high CO coverage, the Ni(100) and Ni(111)

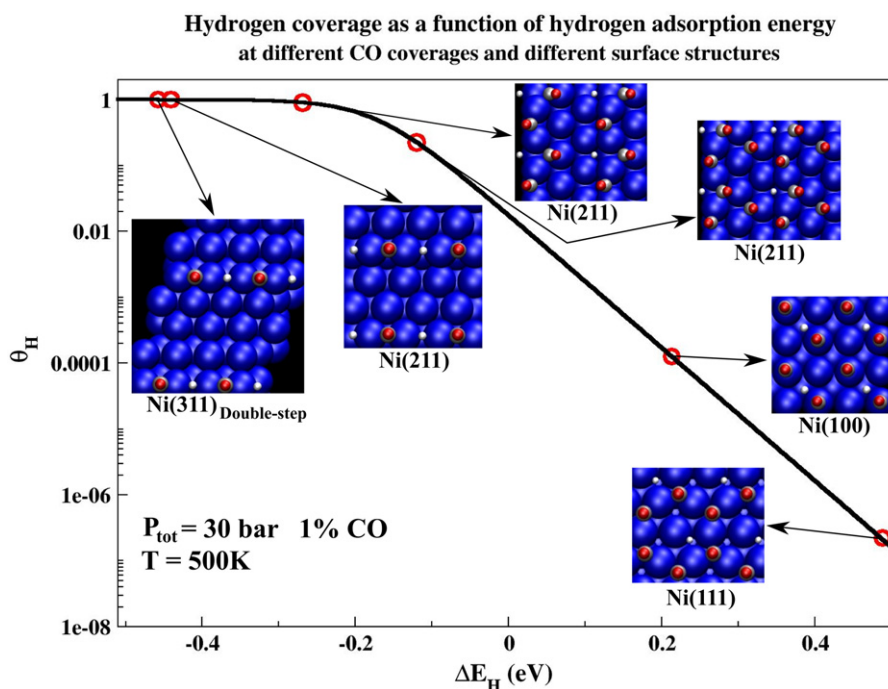


Fig. 7. Calculated hydrogen coverage on Ni at conditions relevant for the methanation reaction as a function of the hydrogen adsorption energy. At steps, the H coverage can be large even at high CO coverages whereas the H coverage is very low on the (111) and (100) surfaces. Carbon atoms are shown grey, hydrogen white, oxygen red, and Ni surface atoms blue. (For interpretation of the references to color in this figure legend the reader is referred to the web version of this article.)

surfaces will have very low H coverage due to repulsive interactions with the CO. The repulsive interaction also manifests itself in a much higher barrier for H₂ dissociation on the CO covered Ni(100) surface (1.9 eV) making H₂ dissociation rate limiting and thereby blocking the COH route under methanation conditions. We note that the steps and edges have no problems in terms of access to co-adsorbed H (see Fig. 7).

3. UHV experiments

To experimentally investigate the dissociation of CO on a well-defined model system, a Ni(14 13 13) single crystal was used. The surface consisted of (111) terraces with an average width of approximately 26 atomic rows, separated by monoatomic steps with (100) facets. The step density was approximately $4 \pm 0.5\%$. The crystal (supplied by Metal Crystals and Oxides Ltd.) was 10 mm in diameter. Sample preparation and reactivity measurements were done in an UHV apparatus as described in Ref. [12]. In recent studies, we found that even remote amounts of nickel carbonyl [Ni(CO)₄] can act as highly active reaction centers and thus have a dramatic effect on surface reactivity [32]. Thus, we took great care to avoid the presence of nickel carbonyls on the surface, by passing the CO gas first through a copper coil heated to 373 K and then through another copper coil loaded with zeolite cooled to the temperature of liquid nitrogen, as suggested by Yates [50]. Furthermore, the tube leading to the leak valve was made of copper, and the CO purification system was pumped out with a turbo pump between the CO doses. The CO purification system is filled with CO only immediately before dosing and only to a low pressure, because carbonyl formation is strongly pressure-dependent. Reducing the time that CO is in the tube after purification further limits possible nickel carbonyl formation through contact with the two stainless steel valves. We found that careful cleaning of the CO as described above was necessary to avoid adsorption of nickel carbonyls on the surface.

The CO was dosed at 500 K. To achieve very accurate measurements of amounts down to 0.005 ML, we used titration of the adsorbed carbon with oxygen followed by TPD, as described previously [12].

Fig. 8 shows carbon uptake curves as a function of CO exposure on the clean and modified surfaces precovered with 0.05 ML sulfur. The insert illustrates the effect of adding sulfur to the surface. Clearly, adding even small amounts of sulfur has a dramatic effect on the surface reactivity. Slightly more than 0.03 ML of sulfur was needed to fully poison the surface, but taking into account the uncertainties of the step density and the coverage determination, this value could easily vary by as much as ± 0.01 ML. Previous studies have clearly shown that sulfur preferentially bonds to the steps [12]; this finding has also been supported by STM investigations [31]. Adding 0.05 ML of sulfur (with a step density of only 0.04) ensured that the steps were completely blocked, which completely deactivated the surface. This suggests that at UHV conditions, the undercoordinated steps or kink sites are the only active sites for dissociating CO.

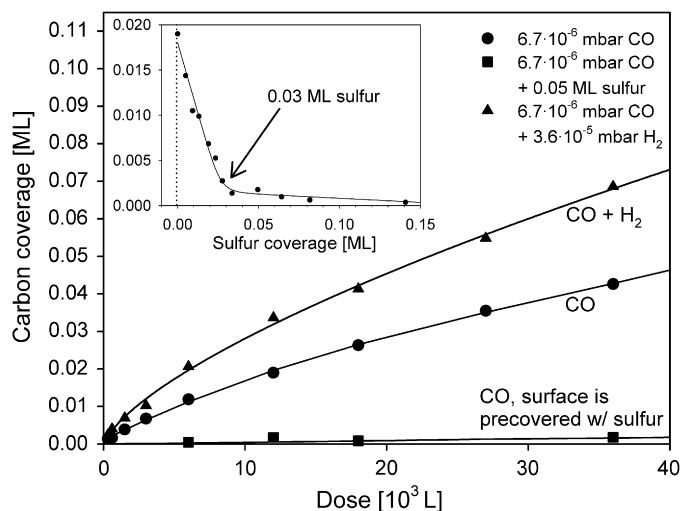


Fig. 8. Experimentally determined carbon coverage on Ni(14 13 13) as a function of CO exposure at 500 K ($1 \text{ L} = 1.33 \times 10^{-6}$ mbars), for a clean surface with exposed steps (circles) and a surface precovered with 0.05 ML sulfur to block the steps (squares). The insert shows the carbon deposition as a function of sulfur coverage for repeated doses at 6.7×10^{-6} mbar CO at 500 K. The carbon uptake beyond 0.03 ML is probably due to incomplete poisoning of steps along the rim of the crystal where a much higher density is expected. The effect of adding hydrogen is observed to enhance the CO dissociation rate. See text for discussion.

For the surfaces on which the active steps sites are available, the activation barrier for CO dissociation can be estimated from the uptake curves given in Fig. 8. The initial rates of carbon uptake were 1.3×10^{-5} ML/s for the clean surface and 2.2×10^{-7} ML/s for the sulfur-covered surface, respectively. Assuming a simple first-order dissociation process, the activation energy can be given as

$$E_a = -k_B T \cdot \ln\left(\frac{r}{0.04\nu\theta_{\text{CO}}}\right), \quad (1)$$

where $k_B = 1.381 \times 10^{-23}$ J/K is the Boltzmann constant, $T = 500$ K is the applied temperature, r is the reaction rate, ν is the pre-exponential factor (we assume a standard value of 10^{13} s^{-1}), 0.04 is the approximate density of steps on our surface, and θ_{CO} is the coverage of CO along the step. Based on the DFT calculations of the CO coverage along the step as reported in the phase diagram in Fig. 5, a value of 0.02 was found for the step coverages at the pressures used in the experiment, which, using Eq. (1), gives an activation barrier of 1.5 eV. If instead the CO step coverage were estimated from the experimentally determined desorption energy of 1.24 eV from Ref. [33], then the CO coverage on the step would be 0.2 (incoming CO flux at 300 K), and the activation energy, again using Eq. (1), would be 1.6 eV. The C-uptake was also measured at $p = 1.3 \times 10^{-6}$ mbar, yielding an initial rate of 3.3×10^{-6} ML/s, similarly leading to activation energies of 1.5 and 1.6 eV, because the coverages will adjust accordingly. These values are in good agreement with the DFT values of 1.7–1.9 eV found for CO dissociation at low-coordinated sites at low CO coverage.

To investigate the influence of H₂ under the UHV conditions, we also studied various CO exposures in a background

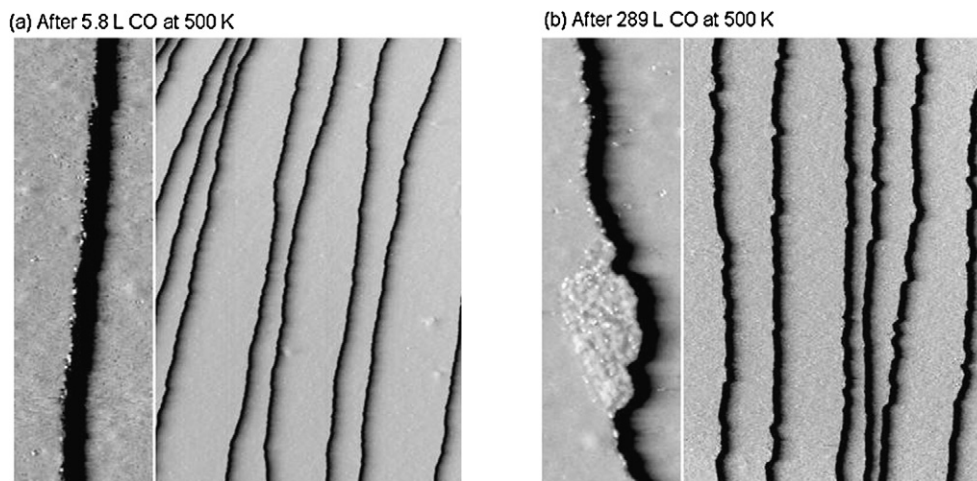


Fig. 9. STM images of atomic steps on a Ni(111) single crystal after different CO exposures at 500 K. All images are recorded in constant current mode with image sizes of $3400 \times 5000 \text{ \AA}$ (insert to the left: $220 \times 700 \text{ \AA}$). The exposures were 5.8 L (a) ($p = 3 \times 10^{-7}$ mbar) and 289 L (b) ($p = 4 \times 10^{-5}$ mbar), respectively. No carbon is seen on the terraces in both cases, and carbon in the form of carbide is only seen in (b) along the steps. The carbide island is clearly seen in the enlarged insert in (b).

of hydrogen. The experimental setup allowed dosing of CO in a background of H_2 only up to 3.6×10^{-6} mbar. Nevertheless, an increase in the initial CO dissociation rate on clean Ni of 1.7 was observed. Dosing H_2 alone (not shown) did not lead to any carbon deposits, as expected; thus, a cooperative effect indeed could be the origin of this effect, as we discuss later.

To further substantiate the calculated and experimentally measured high value for the barrier for CO dissociation, we performed STM measurements on a Ni(111) single crystal. The CO gas was carefully purified in a procedure similar to the experiments reported in Fig. 8. CO was dosed with all filaments turned off to avoid dissociation of CO on the filaments. A magnetron was used to monitor the pressure.

Dosing CO at 400 K after careful precautions were taken to avoid the presence of nickel carbonyl, $\text{Ni}(\text{CO})_4$, in the CO gas used for dosing and subsequently investigating the surface by STM, we were unable to reproduce the results reported by Nakano et al. [28] and Lauritsen et al. [31], who found that CO dissociated at the steps at this temperature. Thus, no dissociation products were observed in this work after exposure at 400 K [32]. However, we did observe some dissociation at 500 K (Fig. 9), in agreement with the observations of Nakano et al., who reported a somewhat higher rate at this temperature [29,30]. After dosing the CO at different pressures and exposure times at temperatures around 500 K, the sample was allowed to cool to room temperature, at which point STM images were obtained (see Fig. 9; details of the step are shown in the inserts). After a low exposure of CO (5.8 L), no or very little carbide was formed on the surface, and then only along the steps. After higher exposures (289 L), carbide islands formed at the upper step edge, but no carbide was seen on the terraces. These findings are also clearly in agreement with the DFT results indicating that only undercoordinated sites were active for the CO dissociation and also reasonably in line with the measured carbon uptake shown in Fig. 8. The carbon formed at the step is expected to grow carbidic islands nucleating along the steps, similar to the results of ethylene exposure

on Ni(111) investigated by STM [51] and further supported by DFT [52].

4. High-pressure experiments

We now consider high-pressure experiments for the methanation reaction. We followed previous kinetic analysis [35] and the DFT calculations [40] in analyzing the results, assuming that the CO(H) dissociation step is the RLS. We tested the two main conclusions from the DFT results at high CO pressures: The reaction site is an undercoordinated site, and the affect of hydrogen is instrumental in the methanation reaction.

The experiment was performed on supported nickel particles under realistic methanation conditions at much higher pressures than those applied in the experiments shown in Fig. 8. The reaction site was investigated by correlating the rate of methanation of CO per Ni mass with the average nickel particle diameter, d . In this method, the activity will scale with the number of active sites, and if these are the surface atoms on the facets of the particles, then the activity will scale with $1/d$ for the relative large particle sizes used here. This is the situation termed “structure insensitive” by Boudart: “The TOF under fixed conditions does not depend or depends only slightly on surface crystalline anisotropy as expressed on clusters of varying size or on single crystals exposing different faces” [53]. If the active sites are on the edge, then scaling with $(1/d)^2$ will be expected, and, finally, if the active site is on corner-like sites, then the scaling will be with $(1/d)^3$. Kink sites may also scale by $(1/d)^3$, because the number of kink sites in the lowest-energy configuration of a nickel particle is affected by the fact that the number of atoms in the particle do normally not match the number of atoms in a regular particle shape. Thus, the number of kink sites does not change much with particle size, resulting in a scaling factor for kinks of $(1/d)^3$.

The data given in Ref. [54] were reanalyzed to determine the scaling factor between methanation activity and nickel particle size for a nickel methanation catalyst (MCR-2X, Haldor

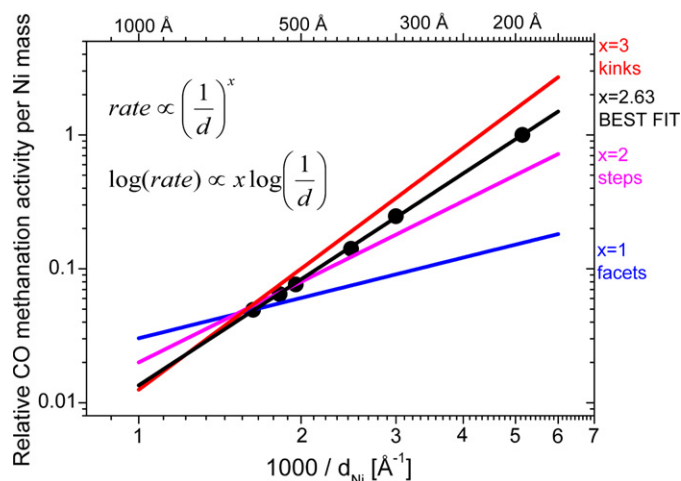


Fig. 10. Measurements of the relative rate of CO methanation activity per Ni catalyst mass plotted as a function of the inverse particle size, d , for a series of nickel catalysts. The methanation reaction is measured in 1% CO in H_2 at 523 K and a total pressure of 1 bar. Note that both axes are logarithmic. It is seen that the measurements (black circles) are best described by an exponent of 2.6, which is in between exponents expected for steps and kinks, suggesting that the reaction is structure sensitive, and that the highly under-coordinated sites are the active sites for the methanation reaction.

Topsøe A/S). The catalyst was initially aged at 600 °C for up to 8450 h in an equilibrated synthesis gas mixture, as described in more detail previously [54]. After aging, the nickel surface areas of the catalyst samples were determined by hydrogen chemisorption at 298 K assuming $H/Ni = 1$ and a Ni area of $A_{Ni} = 6.5 \times 10^{-20} \text{ m}^2$ [55]. The rates of CO methanation at 523 K (1% CO in H_2) were obtained as described previously [9]. Nickel surface areas can be converted to average nickel particle diameters assuming a simple particle shape, resulting in

$$d_{Ni} (\text{Å}) = 68.2 \frac{X_{Ni} (\text{wt}\%)}{A_{Ni} (\text{m}^2 \text{g}^{-1})}, \quad (2)$$

where X_{Ni} is the amount of Ni per catalyst weight (in %) and A_{Ni} is the measured Ni surface area per catalyst weight.

Fig. 10 plots the measured relative rates of methanation per Ni mass as a function of $(1/d)$. Note that both axes are logarithmic, and thus the slope contains information on the type of reaction site. The plot shows that the measured relative methanation activities and $(1/d)$ are proportional. The slope of the best linear fit to the data is 2.6, suggesting that undercoordinated sites such as steps and edges (slope of two) and kinks and corners (slope of three) dominate the observed activity. Thus, the data in Fig. 10 indicate that atomic terraces are inactive for methanation, whereas undercoordinated surface sites are active. This observation supports the conclusions from the DFT calculations and single-crystal measurements that methanation is a highly structure-sensitive reaction. We discuss the effect of hydrogen on the rate in the next section.

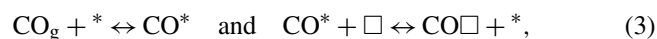
5. Discussion

Our experiments under UHV conditions suggest that the barrier for CO dissociation is much lower on steps/defects than

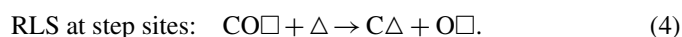
on the terrace (experiments, 1.5–1.6 eV; DFT, 1.7–1.9 eV) and that the barrier is always higher than the barrier for desorption (1.2 eV). Thus, no dissociation would be expected during a TPD experiment if the CO were carefully cleaned for impurities, such as nickel carbonyls.

Turning now to the observed activation energies and effect of hydrogen during the methanation reaction, we need to compare the kinetics for the situations in which CO dissociation is the RLS and in which a COH species is the RLS. If we assume that the methanation reaction is rate-limited by CO dissociation, then a simple model would comprise the following steps:

Quasi-equilibrium: $CO_g + \square \leftrightarrow CO\square$ and



and



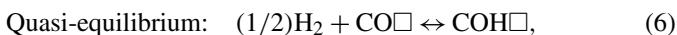
Here *, \square , and Δ denote adsorption sites on the terrace, the upper step/edge, and the lower step/edge site, respectively. The CO adsorbed on the upper step/edge sites naturally will be in equilibrium with the CO adsorbed on the terrace sites, but because the barrier for dissociation is much higher on the terrace, only dissociation on the edge sites are considered in Eq. (4). As discussed earlier, the empty site below the step/edge site denoted Δ adsorbs CO and hydrogen weakly (−0.45 eV) when CO is sitting on the upper site and thus can be considered approximately empty and available when the molecule is dissociating. The oxo-compound will occupy the upper site while the carbon will occupy the lower site, from which it either will be hydrogenated or will diffuse into the upper terrace and nucleate into a carbide island, as demonstrated by STM. Equation (4) would lead to a (forward) methanation rate determined solely by the CO dissociation rate and the coverage of CO on the edge sites, θ_{CO} ,

$$r = k_{\text{diss}}^{\text{CO}} \theta_{CO} \theta_{\Delta} \cong k_{\text{diss}}^{\text{CO}} \theta_{CO}, \quad (5)$$

where $k_{\text{diss}}^{\text{CO}}$ is the reaction rate constant for the RLS. According to the phase diagram in Fig. 5, the surface is expected to be dominated by adsorbed CO under methanation conditions, and the reaction order in CO is indeed observed to be negative for CO pressures above a few mbar [8,34,56], because under such conditions, CO will block the lower step/edge sites and surface sites for H_2 adsorption, for example. At the high pressures used under methanation conditions, the negative reaction order for CO (if any) will lead to higher activation energy for the CO dissociation compared with that measured under UHV conditions and no significant dependence on the hydrogen, which binds weakly compared with CO. Therefore, the mechanism specified in Eqs. (4) and (5) is not relevant for methanation conditions, because the barrier for direct CO dissociation is far too high (1.5–1.8 eV) and will only become higher when the blocking also is considered.

We now investigate the effect of hydrogen present at higher pressures. This opens up the possibility that CO reacts through a COH intermediate formed from adsorbed CO and H. If we assume that the following reaction is in equilibrium on the edge

sites,



then the coverage of COH on the edge can be found as

$$\theta_{\text{COH}} = K_{\text{COH}\leftrightarrow\text{CO}\square+(1/2)\text{H}_2} \sqrt{P_{\text{H}_2}} \theta_{\text{CO}}, \quad (7)$$

where $K_{\text{COH}\leftrightarrow\text{CO}\square+(1/2)\text{H}_2}$ is the equilibrium constant for the reaction in Eq. (6). The RLS now becomes the dissociation of COH instead of CO, as was the case in Eq. (4),



The rate of carbon formation can now be written as

$$r = k_{\text{diss}}^{\text{COH}} \cdot \theta_{\text{COH}} \cdot \theta_{\Delta} \approx k_{\text{diss}}^{\text{COH}} \cdot \theta_{\text{COH}}, \quad (9)$$

where $k_{\text{diss}}^{\text{COH}}$ is the rate constant for the dissociation in Eq. (8) over an edge site. The coverage of free neighbor sites below the step/edge (Δ) is assumed to be close to 1 for the same reasons as before. Inserting Eq. (7) into Eq. (9) gives

$$r \approx k_{\text{diss}}^{\text{COH}} \cdot K_{\text{COH}\leftrightarrow\text{CO}\square+(1/2)\text{H}_2} \sqrt{P_{\text{H}_2}} \theta_{\text{CO}}. \quad (10)$$

The rate is seen to be half-order in hydrogen. The equilibrium constant, $K_{\text{COH}\leftrightarrow\text{CO}\square+(1/2)\text{H}_2}$, can be expressed as

$$\begin{aligned} K_{\text{COH}\leftrightarrow\text{CO}\square+(1/2)\text{H}_2} &= \exp\left(\frac{-\Delta G_{\text{COH}\leftrightarrow\text{CO}\square+(1/2)\text{H}_2}}{k_{\text{B}}T}\right) \\ &= \exp\left(\frac{-\Delta H_{\text{COH}\leftrightarrow\text{CO}\square+(1/2)\text{H}_2}}{k_{\text{B}}T}\right) \\ &\quad \times \exp\left(\frac{\Delta S_{\text{COH}\leftrightarrow\text{CO}\square+(1/2)\text{H}_2}}{k_{\text{B}}}\right), \end{aligned} \quad (11)$$

where k_{B} is the Boltzmann factor, T is the temperature, $\Delta H_{\text{COH}\leftrightarrow\text{CO}\square+(1/2)\text{H}_2}$ is the enthalpy change, and $\Delta S_{\text{COH}\leftrightarrow\text{CO}\square+(1/2)\text{H}_2}$ is the entropy change for Eq. (6). The enthalpy can be written as

$$\Delta H_{\text{COH}\leftrightarrow\text{CO}\square+(1/2)\text{H}_2} = \Delta H_{\text{COH}} - \Delta H_{\text{CO}} - \frac{1}{2} \Delta H_{\text{H}_2}, \quad (12)$$

and the entropy can be written as

$$\Delta S_{\text{COH}\leftrightarrow\text{CO}\square+(1/2)\text{H}_2} = \Delta S_{\text{COH}} - \Delta S_{\text{CO}} - \frac{1}{2} \Delta S_{\text{H}_2}. \quad (13)$$

The rate constant for the RLS, $k_{\text{diss}}^{\text{COH}}$, also can be split up in a similar manner as the equilibrium constant,

$$\begin{aligned} k_{\text{diss}}^{\text{COH}} &= \frac{k_{\text{B}}T}{h} \exp\left(\frac{-\Delta E_{\text{diss}}}{k_{\text{B}}T}\right) \exp\left(\frac{\Delta S_{\text{diss}}}{T}\right) \\ &\cong \frac{k_{\text{B}}T}{h} \exp\left(\frac{-(\Delta H_{\text{COH}_{\text{TS}}} - \Delta H_{\text{COH}})}{k_{\text{B}}T}\right), \end{aligned} \quad (14)$$

where h is Planck's constant, $\Delta E_{\text{diss}} = \Delta H_{\text{COH}_{\text{TS}}} - \Delta H_{\text{COH}}$ is the energy difference between the COH in the transition state, COH_{TS} , and the adsorbed COH species on the edge, and $\Delta S_{\text{diss}} = \Delta S_{\text{COH}_{\text{TS}}} - \Delta S_{\text{COH}} \cong 0$, because there is no reason to expect any large difference in degrees of freedom for the two states.

Inserting Eqs. (11)–(14) into Eq. (10), the expression for the rate of COH dissociation from Eq. (8) becomes

$$\begin{aligned} r &\approx \frac{k_{\text{B}}T}{h} \exp\left(\frac{-(\Delta H_{\text{COH}_{\text{TS}}} - \Delta H_{\text{CO}} - (1/2)\Delta H_{\text{H}_2})}{k_{\text{B}}T}\right) \\ &\quad \times \exp\left(\frac{\Delta S_{\text{COH}\leftrightarrow\text{CO}\square+(1/2)\text{H}_2}}{k_{\text{B}}}\right) \sqrt{P_{\text{H}_2}} \theta_{\text{CO}}. \end{aligned} \quad (15)$$

Because ΔH_{COH} cancels as the COH intermediate is assumed in equilibrium, the energy difference ($\Delta H_{\text{COH}_{\text{TS}}} - \Delta H_{\text{CO}} - (1/2)\Delta H_{\text{H}_2}$) is exactly that estimated through the DFT calculations earlier: $E_{\text{a,COH}} = E_{\text{Transition state}} - E_{\text{CO ads.}} - (1/2)E_{\text{H}_2 \text{ gas}}$. Here the lowest barrier was found to be 1.08 eV for dissociation of COH on an edge site. Inserting this, we get

$$\begin{aligned} r &\approx \left[\frac{k_{\text{B}}T}{h} \exp\left(\frac{\Delta S_{\text{COH}\leftrightarrow\text{CO}\square+(1/2)\text{H}_2}}{k_{\text{B}}}\right) \right] \\ &\quad \times \sqrt{P_{\text{H}_2}} \theta_{\text{CO}} \left(\frac{-E_{\text{a,COH}}}{k_{\text{B}}T} \right) \\ &= \nu \sqrt{P_{\text{H}_2}} \theta_{\text{CO}} \exp\left(\frac{-E_{\text{a,COH}}}{k_{\text{B}}T}\right) \\ &= (\nu^* \theta_{\text{active sites}}) \sqrt{P_{\text{H}_2}} \theta_{\text{CO}} \exp\left(\frac{-E_{\text{a,COH}}}{k_{\text{B}}T}\right), \end{aligned} \quad (16)$$

where ν is introduced as the prefactor and ν^* as the prefactor per active site. This P_{H_2} dependence has indeed been reported in the literature for a gas mixture of 0.9% CO in H_2 when increasing total pressure in the range of 25–100 bar [57], whereas the reaction order was smaller for pressures <25 bar. To estimate the reaction order in CO, we again consider the rate given in Eq. (9), this time maintaining θ_{Δ} . By inserting the relevant expressions for θ_{CO} and θ_{Δ} into the definition of the reaction order ($n_{\text{CO}} \equiv P_{\text{CO}}(\partial \ln r^+ / \partial P_{\text{CO}})$), we find that $n_{\text{CO}} = 1 - \theta_{\text{CO}\square} - \theta_{\text{CO}\Delta} \cong -\theta_{\text{CO}\Delta}$, giving rise to an only slightly negative reaction order in CO, because, as mentioned earlier, the CO molecule is much more weakly bonded at the lower step site. This is consistent with findings of Vannice [8,34] of slightly negative exponents (−0.3 to −0.5) for CO partial pressure and positive exponents for hydrogen partial pressure (0.6 to 0.8) at around 1 bar. Similar data were reported by Baerns et al. [37] and Harriott et al. [38], with a small negative order in CO pressure and a somewhat higher positive order for hydrogen, resulting in a small overall positive reaction order of the total pressure (0–0.5). This seems to be the general picture, but there are substantial variations in these results. Consequently, we refrain from providing further details on the reaction order here, but nonetheless do speculate that the slightly negative effect of CO can be ascribed to a blocking of the surface by adsorbed CO on the lower step edge site, whereas a hydrogen exponent >0.5 can be ascribed to removal of carbon, which is known to poison the surface, particularly at low hydrogen pressures [5,6]. The role of carbon poisoning is discussed in the Appendix A.

The mechanism proposed here predicts a low prefactor due to the entropy loss shown in Eq. (6). The entropy change can be found from DFT calculations by inserting the following into Eq. (13):

$$\begin{aligned} \Delta S_{\text{CO-COH}} &= \Delta S_{\text{COH}} - \Delta S_{\text{CO}^*} - \frac{1}{2} \Delta S_{\text{H}_2} \\ &= 27.0 - 32.8 - 57.9 = -63.7 \text{ J/(mol K)}, \end{aligned} \quad (17)$$

resulting in a value for the prefactor of $\nu = \nu^* = 4.9 \times 10^9 \text{ s}^{-1}$. The activation energy is $E_{a,\text{COH}} = 1.08 \text{ eV}$, as found by DFT and reported in Fig. 4 for activation through the COH complex.

From measurements on supported Ni catalysts, Sehested et al. [35] found a prefactor of $\nu = 2.0 \times 10^8 \text{ s}^{-1}$ and $E_{\text{diss}} = 1.01 \text{ eV}$ when calculated at the reaction conditions ($P_{\text{H}_2} = 1.37 \text{ bar}$ and $P_{\text{CO}} = 0.028 \text{ bar}$). Taking into account the number of active sites relative to the total number of surface sites (estimated experimentally as 0.05 [35]), the prefactor on a per active site basis becomes $\nu^* = 4.0 \times 10^9 \text{ s}^{-1}$ [see Eq. (16)], in excellent agreement with these model predictions.

Goodman et al. [5] measured methanation rates on a Ni(100) single crystal (and similar data on Ni(111) [6]) and found rates of 1 s^{-1} for $P_{\text{H}_2} = 0.128 \text{ bar}$ and $P_{\text{CO}} = 0.032 \text{ bar}$ at 650 K. The prefactor was determined to be $\nu = 5.3 \times 10^8 \text{ s}^{-1}$, and an activation energy of 103 kJ/mol ($E_{\text{diss}} = 1.07 \text{ eV}$) can be derived [5–7,41]. Here it is assumed that all of the surface terrace atoms on the front and back sides of the single crystal are contributing to the reaction. It is seen that the prefactor compares well with the value from the model prediction and the experimental data on the Ni catalyst described above [35] if a defect density of 10% on the single crystal surface is assumed. This may seem a rather high value when considering that the Ni(100) was polished on both sides, with 1–2% defects being a realistic estimate [15]. Keep in mind, however, that in those experiments, the surface atoms on the rim of the crystal and the surface close to the rim edges (which are always less well defined) contributed to the reaction, as did the wires for supporting and heating the crystal, which were also made of Ni [5]. Given these considerations, an overall defect density of 10% is not an unrealistic estimate. Note that DFT predicted a low barrier height of 1.08 eV for the double steps (D4) but a barrier height of 1.3 eV for the single steps, quite close in energy (B_4^{COH}).

Using Eq. (16), we can estimate the expected hydrogen enhancement on the CO dissociation during the UHV experiment shown in Fig. 8. Using a partial pressure of $P_{\text{H}_2} = 3.6 \times 10^{-8} \text{ bar}$ and a CO coverage of 0.2 ML on the step, we find a rate of $1 \times 10^{-7} \text{ ML/s}$, which is roughly a factor of 200 less than the rate enhancement observed. Therefore, our measured rate enhancement must come from another mechanism. One possibility is that hydrogen helps remove oxygen from the dissociated CO and thereby frees steps for the simple CO dissociation. The oxygen is usually removed by CO to form CO_2 . Previous experiments performed by Alstrup et al. [58] showed that the hydrogenation of adsorbed carbon is rather slow at low pressures of hydrogen (i.e., <1 mbar) but becomes significant at higher pressures and proceeds with an exponent >1, and thus will be much faster than the CO dissociation at elevated pressures discussed earlier. Unfortunately, studying the effects of higher hydrogen pressures in the UHV setup used in this study was not possible.

Based on the foregoing comparisons, we can conclude that there is excellent agreement between experimental rate data from both single crystals and supported catalysts and a relative simple model in which the reactivity will always be completely dominated by defect sites due to the large difference in activation energy between, for instance, step sites and terrace sites.

Goodman and co-workers [5–7] found that the rate of methanation was roughly the same on Ni(111) and (100), similar (per surface area) to that of supported catalysts. In later work, Kelley and Goodman studied ruthenium [6,41] and found that the methanation rate was the same on Ru(001) and Ru(110) as on Ni, suggesting that the measured rate depends on a delicate balance between carbide formation and carbide hydrogenation on the surface. We agree with that conclusion in the sense that carbide removal eventually will be rate-limiting at a sufficiently low hydrogen-to-CO ratio and particularly at low pressures as used in previous studies [5,6,41] (also see Appendix A). We argue, however, that at higher pressures and at temperatures reasonable for the methanation process, the reaction is rate limited by COH dissociation. If the hydrogenation of deposited carbon were rate-limiting, it would be in disagreement with both the energy diagram calculated by DFT in the present work and the isotope scrambling experiments of Coenen et al. [38]. Similarly, if direct CO dissociation were rate-limiting, it would be in conflict with the present results from DFT, single-crystal experiments, and catalyst measurements. The COH intermediate suggested by DFT calculations is in agreement with earlier work, in which the evidence was rather circumstantial, however [38,39].

The most plausible explanation for the apparent structure-insensitivity of the earlier single-crystal studies is that the reaction is so structure-sensitive that only certain defects can contribute to the measured rates, and the defect density is similar for different samples. This also offers an excellent explanation for the very strong poisoning observed by Goodman and co-workers when adding small amounts of sulfur to the surface [6]. How a single sulfur atom can influence up to 8–10 nickel atoms has long been puzzling, because electronic screening is known to reduce such effects to smaller scales; however, this can be readily understood when, for example, only atomic steps are active, as can be concluded from Fig. 8. CO dissociation is similar to N_2 dissociation, for which UHV experiments found that different Ru single crystal surfaces had the same rates of dissociation [59]. Later DFT calculations and UHV experiments proved that steps completely control the reactivity [15], a conclusion also consistent with the experiments on different single-crystal surfaces.

The present work emphasizes the need for high-pressure experiments on well-defined systems consisting of single crystals in which the composition of surface sites is controlled and, for example, the rim of the crystal and the heating support can be eliminated. This work, currently in progress, poses a substantial experimental challenge.

6. Summary and conclusions

We have provided evidence based on DFT calculations, carbon uptake, and STM experiments indicating that steps are the primary active sites for CO dissociation on clean Ni(111) surfaces. No dissociation was observed over closely packed Ni atoms on the terraces. Experimentally, the barrier over a step site under UHV conditions was found to be 1.5–1.6 eV. This is in good agreement with DFT studies that found values of

1.7–1.9 eV over an undercoordinated site on the Ni surface. All values exceed the desorption energy of CO (previously found to be 1.2 eV), in agreement with the fact that no CO dissociation was observed during TPD when the gas was appropriately cleaned. When including the effect of hydrogen present under methanation conditions, a different transition state was found that involves dissociation through a COH species. In this case, the barriers were 1.08 eV for edges/double steps and 1.3 eV for steps, values that are in excellent agreement with previous measurements of the methanation reaction that found activation energies of 1.01 eV for supported catalysts and 1.08 eV for single crystals. Correlations of methanation activity with the particle size of supported Ni catalysts support the characterization of the reaction site as an undercoordinated surface site. Furthermore, the proposed reaction mechanism with the COH intermediate resulted in a square root dependence of the hydrogen pressure, in agreement with literature findings at high pressure. Our results, largely summarized in Fig. 6, show that for pressures and temperatures appropriate for the methanation reaction, dissociation of a COH intermediate on step/edge site is the RLS. The difference in the reaction mechanism under UHV and methanation conditions clearly demonstrates the importance of combining surface science techniques with *ab initio* calculations when bridging the pressure gap.

Acknowledgments

The authors thank J.T. Yates for his critical review of the manuscript. M.P.A. and F.A.P. were supported by the Danish Research Agency (grant 26-04-0047). M.P.A. was supported by a Marie Curie fellowship (EU grant MEIF-CT-2004-011121). The DFT calculations were performed with support from the Danish Center for Scientific Computing (grant HDW-1103-06). CINF is funded by the Danish National Research Foundation. CAMD is funded by the Lundbeck Foundation.

Appendix A

In several earlier works on both real catalysts [60] and single crystals [5–7,41], poisoning by carbon was observed when the hydrogen pressure relative to the CO pressure was too low to ensure sufficiently rapid removal of the formed carbon by hydrogen. For instance, Goodman et al. reported that the methanation rate correlates inversely with the amount of carbide measured on the surface after experiments at 625 K at pressures of 1–2000 mbar [6,41]. The carbide coverage measured after non-Arrhenius behavior at low pressure rose up to 0.25 ML at 1.3 mbar but remained rather constant, at around 0.05 ML, when measured after Arrhenius behavior [41]. It can be speculated that this low level does not reflect the level under reaction conditions, but rather that the crystal has an even lower coverage of carbon under the Arrhenius conditions, whereas the observed carbon is deposited as the reactants are pumped out. Nevertheless, it is clear that deposition of large amounts of carbon on the surface will eventually poison the steps; however, as shown in Fig. 9, the carbon agglomerates into carbide islands and does not decorate the steps at low coverage, as, for

instance, sulfur does [12,31]. Thus, carbon is not expected to be an efficient poison for the methanation process.

Moreover, several studies on the hydrogenation of carbon on Ni have clearly indicated that the hydrogenation rate due to lack of hydrogen eventually becomes rate-limiting. It has been speculated that this may be the origin of the observed lack of structure sensitivity [61]; however, this phenomenon likely will be of importance only at very low hydrogen pressures or at high temperatures, as shown in Fig. 6. To elucidate this, we created a very simple model assuming that the carbon coverage at the steps is determined by a carbide formation rate given by the dissociation rate derived in Eq. (16) and a carbide removal rate determined by a hydrogenation rate. The hydrogenation rate is extracted from the work of Alstrup et al. [58], who found that the rate is basically temperature-independent around 500 K, whereas the reaction order in hydrogen is 1.7 in the pressure regime of 0.5–13 mbar and is given by

$$r_{\text{Hyd}} = 54 \cdot P_{\text{H}_2}^{1.7} \left(\frac{\text{ML carbon}}{s} \right) \quad (18)$$

at saturation coverage. It is assumed that this rate is a good description of what is occurring at the steps.

With this, we can set up the following equations assuming steady state:

$$\frac{d\theta_{\text{C}}}{dt} = 0 = r_{\text{diss-COH}}(1 - \theta_{\text{C}}) - r_{\text{Hyd}}\theta_{\text{C}} \Rightarrow$$

$$r_{\text{CH}_4} = r_{\text{diss-COH}}(1 - \theta_{\text{C}}) = r_{\text{diss-COH}} \frac{r_{\text{Hyd}}/(r_{\text{diss-COH}})}{1 + r_{\text{Hyd}}/(r_{\text{diss-COH}})}, \quad (19)$$

where θ_{C} is the carbon coverage at the step and it is assumed that a step site is available as long as it is not covered by carbon.

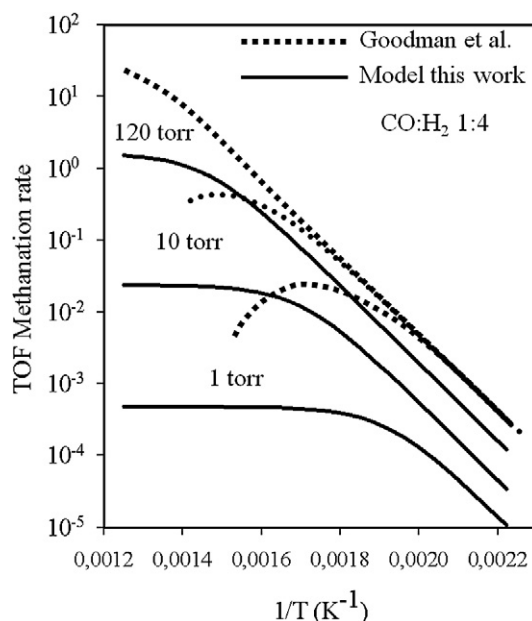


Fig. 11. Comparison between the experimental data obtained on Ni(100) [5, 6] and the present model where carbon poisoning is taken into account. The absolute values are only quantitatively in agreement for the higher pressures while larger deviations are observed for lower pressures. Note, however, that the model captures qualitatively the onset of carbide poisoning of the steps although it is not taking the formation of islands into account.

$r_{\text{diss-COH}}$ is given by Eq. (16). To keep things simple, the model does not include island formation.

The resulting rates are then depicted in an Arrhenius plot in Fig. 11, allowing a comparison to the experimental data of Goodman et al. [5]. It is obvious that our data do not fit the experimental rates quantitatively, especially for the low pressures, because our dissociation rate is dependent on hydrogen pressure. However, the qualitative trends are in very good agreement, demonstrating the poisoning of carbon when the hydrogenation rate cannot keep up with the dissociation rate, leading to deviations from the Arrhenius behavior at higher temperatures, especially at low pressure. Obviously, the carbon poisoning will not be a problem at realistic pressures and at temperatures that are kept low for thermodynamic reasons.

References

- [1] P. Sabatier, J.B. Senderens, C. R. Acad. Sci. Paris 134 (1902) 514.
- [2] I. Chorkendorff, H. Niemantsverdriet, Wiley-VCH, Weinheim, ISBN 978-3-527-31672-4, 2007.
- [3] A. Harms, B. Høhlein, E. Jørn, A. Skov, Oil Gas J. 78 (1980) 120.
- [4] M. Dry, Appl. Catal. A Gen. 276 (2004) 1.
- [5] D.W. Goodman, R.D. Kelley, T.E. Madey, J.T. Yates Jr., J. Catal. 63 (1980) 226.
- [6] R.D. Kelley, D.W. Goodman, The Chemical Physics of Solid Surfaces and Heterogeneous Catalysis, Fundamental Studies of Heterogeneous Catalysis, vol. 4, Elsevier Science Publishers, Amsterdam, 1982.
- [7] D.W. Goodman, Acc. Chem. Res. 17 (1984) 194.
- [8] M.A. Vannice, J. Catal. 44 (1976) 152.
- [9] J.R. Rostrup-Nielsen, in: J.R. Anderson, M. Boudart (Eds.), Catalysis Science and Technology, Springer-Verlag, Berlin, 1984.
- [10] T.P. Beebe Jr., D.W. Goodman, B.D. Kay, J.T. Yates Jr., J. Chem. Phys. 87 (1987) 2305.
- [11] J.H. Larsen, I. Chorkendorff, Surf. Sci. Rep. 35 (1999) 163.
- [12] F. Abild-Pedersen, O. Lytken, J. Engbæk, G. Nielsen, I. Chorkendorff, J.K. Nørskov, Surf. Sci. 590 (2005) 127.
- [13] J. Wei, E. Iglesia, J. Catal. 224 (2004) 370.
- [14] T. Zambelli, J. Winterlin, J. Trost, G. Ertl, Science 273 (1996) 1688.
- [15] S. Dahl, A. Logadottir, R.C. Egeberg, J.H. Larsen, I. Chorkendorff, E. Törnqvist, J.K. Nørskov, Phys. Rev. Lett. 83 (1999) 1814.
- [16] Y.K. Kim, G.A. Morgan, J.T. Yates, Surf. Sci. 598 (2005) 14.
- [17] M. Mavrikakis, M. Bäumer, H.J. Freund, J.K. Nørskov, Catal. Lett. 81 (2002) 153.
- [18] I.M. Ciobica, R. van Santen, J. Phys. Chem. B 107 (2003) 3808.
- [19] B. Hammer, Phys. Rev. Lett. 83 (1999) 3681.
- [20] H.S. Bengaard, J.K. Nørskov, J. Sehested, B.S. Clausen, L.P. Nielsen, A.M. Molenbroek, J.R. Rostrup-Nielsen, J. Catal. 209 (2002) 365.
- [21] T. Bligaard, J.K. Nørskov, S. Dahl, J. Matthiesen, C.H. Christensen, J. Sehested, J. Catal. 224 (2004) 206.
- [22] T. Zubkov, G.A. Morgan Jr., J.T. Yates Jr., Chem. Phys. Lett. 362 (2002) 181.
- [23] T. Zubkov, G.A. Morgan Jr., J.T. Yates Jr., O. Kuhlert, M. Lisowski, R. Schillinger, D. Fick, H.J. Janch, Surf. Sci. 625 (2003) 57.
- [24] H. Pfner, P. Feulner, D. Menzel, J. Chem. Phys. 79 (1983) 4613.
- [25] L. Ng, K.J. Uram, Z. Xu, P.L. Jones, J.T. Yates Jr., J. Chem. Phys. 86 (1987) 6523.
- [26] C. Benndorf, L. Meyer, Surf. Sci. 251–252 (1991) 872.
- [27] D.W. Goodman, R.D. Kelley, T.E. Madey, J.M. White, J. Catal. 64 (1980) 479.
- [28] H. Nakano, S. Kawakami, T. Fujitani, J. Nakamura, Surf. Sci. 295 (2000) 454.
- [29] H. Nakano, J. Nakamura, Surf. Sci. 341 (2001) 482.
- [30] H. Nakano, J. Ogawa, J. Nakamura, Surf. Sci. 514 (2002) 256.
- [31] J.V. Lauritsen, R.T. Vang, F. Besenbacher, Catal. Today 111 (2006) 34–43.
- [32] J. Engbæk, O. Lytken, J.H. Nielsen, I. Chorkendorff, Surf. Sci. 602 (2008) 733.
- [33] E. Bjørgum, D. Chen, M.G. Bakken, K.O. Christensen, A. Holmen, O. Lytken, I. Chorkendorff, J. Phys. Chem. 109 (2005) 2360.
- [34] M.A. Vannice, J. Catal. 37 (1975) 449.
- [35] J. Sehested, S. Dahl, J. Jacobsen, J.R. Rostrup-Nielsen, J. Phys. Chem. B 109 (2005) 2432.
- [36] R.Z.C. van Meerten, J.G. Villenbroek, M.H.J.M. de Croon, P.F.M.T. van Nisselroy, J.W.E. Coenen, Appl. Catal. 3 (1982) 29.
- [37] J. Klose, M. Baerns, J. Catal. 85 (1984) 105.
- [38] J.W.E. Coenen, P.F.M.T. van Nisselroy, M.H.J.M. de Croon, P.F.H.A. van Dooren, R.Z.C. van Meerten, Appl. Catal. 25 (1986) 1.
- [39] S. Van Ho, P. Harriott, J. Catal. 64 (1980) 272.
- [40] M.P. Andersson, T. Bligaard, A. Kustov, K.E. Larsen, J. Greeley, T. Johansson, C.H. Christensen, J.K. Nørskov, J. Catal. 239 (2006) 501.
- [41] R.D. Kelley, D.W. Goodman, Surf. Sci. 123 (1982) L743.
- [42] B. Hammer, L.B. Hansen, J.K. Nørskov, Phys. Rev. B 59 (1999) 7413.
- [43] F. Abild-Pedersen, M.P. Andersson, Surf. Sci. 601 (7) (2007) 1747.
- [44] S. Mason, I. Grinberg, A. Rappe, Phys. Rev. 69 (2004) 161401.
- [45] P.J. Feibelman, B. Hammer, J.K. Nørskov, F. Wagner, M. Scheffler, R. Stumpf, R. Watwe, J.A. Dumesic, J. Phys. Chem. B 105 (2001) 4018.
- [46] G. Kresse, A. Gil, P. Sautet, Phys. Rev. 68 (2003) 73401.
- [47] G.A. Morgan Jr., D.C. Sorescu, T. Zubkov, J.T. Yates Jr., J. Phys. Chem. B 108 (2004) 3614.
- [48] O.R. Inderwildi, S.J. Jenkins, D.A. King, J. Am. Chem. Soc. 129 (2007) 1751.
- [49] D.L. Lide (Ed.), CRC Handbook of Physics and Chemistry, 77th ed., Academic Press, London, 1997, and NIST Chemistry web-book, <http://webbook.nist.gov/chemistry/>.
- [50] J.T. Yates Jr., Experimental Innovations in Surface Science, Springer, New York, 1998.
- [51] R.T. Vang, K. Honkala, S. Dahl, E.K. Vestergaard, J. Schnadt, E. Lægsgaard, B.S. Clausen, J.K. Nørskov, F. Besenbacher, Surf. Sci. 600 (2006) 66–77.
- [52] M.P. Andersson, F. Abild-Pedersen, Surf. Sci. 601 (3) (2007) 649.
- [53] M. Boudart, Chem. Rev. 95 (1995) 661.
- [54] J.R. Rostrup-Nielsen, K. Pedersen, J. Sehested, Appl. Catal. A Gen. 330 (2007) 134.
- [55] J.R. Rostrup-Nielsen, Steam Reforming Catalysts, Danish Technical Press, Copenhagen, 1975.
- [56] P. Schoubye, J. Catal. 14 (1969) 238.
- [57] P. Schoubye, J. Catal. 18 (1970) 118.
- [58] I. Alstrup, I. Chorkendorff, S. Ulmann, Surf. Sci. 293 (1993) 133.
- [59] K. Jacobi, H. Dietrich, G. Ertl, Appl. Surf. Sci. 121 (1997) 558.
- [60] M.A. Vannice, R.L. Garten, J. Catal. 50 (1979) 236.
- [61] H. Hirano, K. Tanaka, J. Catal. 133 (1992) 461.